PAPER

Estimation of spectroscopic parameters and TL glow curve analysis of Eu³⁺-activated CaY₂O₄ phosphor

Tirath Ram,[a] Neeraj Verma,[a] Jagjeet Kaur,[a] Abhishek Kumar Misra,[a] Vikas Dubey, [*b] Neha Dubey, [a] Marta Michalska-Domańska, [*c] Janita Saji [d] and Ram Sagar Yadav [e]

The solid-state reaction method was utilised to create a down-conversion phosphor in an air environment in CaY₂O₄:Eu³⁺ nanocrystalline material. The calcination temperature was set at 1000 °C, and the sintering temperature was set at 1300 °C. Following annealing, confirmation of the crystallinity quality of the phosphor was accomplished by the use of X-ray diffraction analysis. The particle size was predicted to be 43.113 nm using Scherrer's formula. To produce down-conversion luminescence spectra, an excitation wavelength of 247 nm was applied with a fluorescence spectrophotometer. The PL got increasingly intense as the concentration of the dopant increased. The maximum intensity was measured at 2.0 mol% of Eu³⁺ ion, which gradually decreased as the concentration increased because of concentration quenching. To analyse spectrophotometric peak determinations, the approach developed by the Commission Internationale de l'Éclairage (CIE) was used. Thermoluminescence (TL) glow curve analysis of the CaY₂O₄:Eu³⁺-doped phosphor manufactured here revealed a wide TL centred at 225 °C, which comprised of so many peaks that may be extracted by the computerised glow curve deconvolution (CGCD) approach using glow-fit software. The associated kinetic parameters were then determined. The prepared phosphor may be useful for application in various display devices upon excitation by 247 nm; the prominent 613 nm peak of the Eu³⁺ ion ($^5D_0 \rightarrow ^7F_2$) electric dipole transition features a red component. CaY₂O₄:Eu³⁺ phosphors show promise as materials for potential use in phosphor-converted white LEDs in the field of solid-state lighting technology. The linear connection that the TL glow curve has with UV dose provides evidence for its possible use in dosimetry.

1. Introduction

Phosphorescence, also known as persistent luminescence (PersL) or long-lasting afterglow, refers to a fascinating occurrence of light emission that persists for several minutes or even hours after the cessation of the initial light excitation, whether it be from UV or visible sources.[1] Long persistent phosphors (LPPs) continue to provoke researchers' curiosity due to their unexplained optical nature and broad applicability. LPPs have found diverse applications in specialised technical fields, such as road signs, decoration, emergency lighting, security displays,

radiation detection, information storage, and imaging displays. These applications have seen increased the utilization of LPPs in recent decades.[2–5] Materials that can store energy in this way also go by the name of electron/hole traps.[6–9] High-energy radiation (*e.g.*, gamma rays, X-rays, or ultraviolet light) creates either electrons or holes, which are then trapped by lattice defects or impurities. After absorbing phonons or infrared photons,[10–14] the bound electrons/holes are slowly freed. Understanding the presence and distribution of these traps presents a significant challenge. It has not been determined yet how charge carriers go from emission centres to traps.[3,15] Lattice imperfections are not just trap centres, but may also act as emission sources.

P. Tadge *et al.* studied the downshifting, frequency up-conversion, and intrinsic optical bi-stability in CaY₂O₄:Ho³⁺/Yb³⁺ and CaSc₂O₄:Ho³⁺/Yb³⁺ phosphors that were synthesised by a complex-based precursor solution method. The X-ray powder diffraction confirmed the formation of highly crystalline phosphors with a pure orthorhombic phase. Fourier transform infrared studies showed vibrational bands and diffuse reflectance spectra. The Ho³⁺/Yb³⁺ co-doped CaSc₂O₄

aDepartment of Physics, Government Vishwanath Yadav Tamaskar Post Graduate Autonomous College, Durg, C.G., India

bDepartment of Physics, North Eastern Hill University (NEHU), Shillong, Meghalaya, 493022, India. E-mail: jsvikasdubey@gmail.com

cInstitute of Optoelectronics, Military University of Technology, Kaliskiego 2, 00-908 Warsaw, Mazovia, Poland

dDepartment of Sciences and Humanities, School of Engineering and Technology CHRIST (Deemed to be University), Bangalore, India

eDepartment of Statistics, Institute of Science, Banaras Hindu University, Varanasi, 221005, India

and CaY$_2$O$_4$ phosphors display intense green downshifting emission upon 454 nm excitations. Their decay curves indicated a non-exponential nature, and the energy transfer microscopic parameters were calculated.[18]

Jeon *et al.* discussed up-conversion to be an anti-stokes process that converted near-infrared light into visible light. CaY$_2$O$_4$ is a promising host material due to its high chemical and thermal stability, low-phonon energy, and environment friendliness. Er^{3+} and Yb^{3+}-doped nano-crystalline phosphors were prepared by a sol–gel process that was characterised by X-ray diffraction and scanning electron microscopy. Photoluminescence properties of the powders were measured by exciting them with a 980 nm diode laser at room temperature. Green and red up-conversion emissions were observed at 520–540 nm, 540–570 nm, and 640–680 nm.[19]

Hwang *et al.* studied the nanocrystalline CaY$_2$O$_4$:Er^{3+} up-conversion phosphor prepared by the sol–gel process. A homogeneous precursor sol was heated on a hot plate; the coagulated gel was pre-fired at 300 °C for 4 h under an Ar atmosphere, followed by final annealing at 1200 °C for 4 h. The crystallinity of the powders after annealing was confirmed using an X-ray diffraction analysis. The shape and particle size of the powders were observed by field emission-scanning electron microscope and transmission electron microscope. The particle size of CaY$_2$O$_4$ powder that had been doped (3 mol%) was homogeneous and varied from 100 to 200 nm, according to micrographic pictures. When Er^{3+} is injected at a 3 mol% doping concentration, up-conversion efficiency is at its maximum. Additionally, the excellent colour purity of the phosphor exhibits colour tunability.[20]

Because of its remarkable thermoluminescence (TL) capabilities, CaY$_2$O$_4$:Eu^{3+} phosphor has been widely recognised as a very effective material for radiation dosimetry. This phosphor exhibits remarkable TL intensity and chemical stability, minimal fading rate, and resistance to environmental variations. Many environmental[16,17] and personnel monitoring[18,19] programs use it. Since the overall energy contained in the phosphor is emitted in a single measurement during the TL readout, any TL reader malfunctioning during measurements would result in a spurious TL readout. TL-grade CaY$_2$O$_4$:Eu^{3+} was found to present photo-stimulated luminescence that varies with the dosage. This discovery holds significant potential for radiation dosimetry as it enables multiple outputs on a phosphor sample that has been exposed to radiation, without significant loss of stored energy.[20] Consequently, this method offers an advantage over the commonly employed TL method, which lacks this capability.

If we can enhance the declining property, a phosphor that is primarily composed of CaY$_2$O$_4$ has the potential to resemble an optimal TL dosimeter material, aside from the issue of tissue equivalence.[21,22]

The phosphors mentioned in this paper are CaY$_2$O$_4$:Eu^{3+}; these newly synthesised phosphors exhibit minimum fading, while retaining nearly all of the other beneficial properties of CaSO$_4$:Mn. Dosimeters are constructed with these phosphors, and their properties are studied from the perspective of radiation dosimetry.[23]

The current research focuses on the creation and analysis of a phosphor material that incorporates Eu^{3+} ions. This synthesised phosphor demonstrates the potential for a wide range of applications, including displays and dosimetry. As the synthesised phosphor features a crystalline quality as per XRD analysis, to study the morphology of the prepared phosphor, SEM analysis was performed; functional group and modes of vibration were studied by FTIR; spectroscopic analysis was performed using PL emission and excitation spectra, while colour optimisation was done through CIE coordinate and trap parameter analysis was conducted using a TL glow curve analysis *via* the CGCD technique.

2. Experimental

A conventional solid-state reaction method was used to manufacture Eu^{3+}-doped CaY$_2$O$_4$ phosphor. Sigma-Aldrich provided high-purity CaCO$_3$, europium oxide (Eu$_2$O$_3$) (0.1–2.5 mol%), and yttrium oxide (Y$_2$O$_3$) (99.9%). The chemicals that were used as precursors were mixed using flux boric acid (H$_3$BO$_3$). The appropriate quantities of these substances were measured out and finely ground using an agate mortar and pestle. The powdered sample was calcined at 1000 °C for an hour using an alumina crucible and then sintered at 1300 °C for 4 h in a muffle furnace. After each round of heating, the sample was ground. The sample was heated to a high temperature in the same furnace and then cooled to room temperature (Fig. 1).[24,35]

$$CaCO_3 + Y_2O_3 \rightarrow CaY_2O_4 + CO_2$$

$$Y_2O_3 + CaCO_3 + Eu_2O_3 \rightarrow CaY_2O_4:Eu^3$$
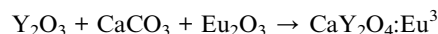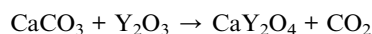
To determine the crystalline quality of the phosphor and its particle size, X-ray diffraction studies were performed (Advanced Bruker D8 from Germany). We used a CuKα source in an X-ray diffractometer to collect data with X-ray powder diffraction analysis. The X-rays, having a wavelength of 0.154 nm, were produced within a hermetically sealed tube. To detect the X-rays, a high-speed silicon strip technology-based detector known as the Bruker Lynx Eye detector was employed (Bruker made in Germany). To ascertain the molecular structure, FTIR analysis was carried out. A Shimadzu RF-5301 PC spectrofluorophotometer was used to obtain both the emission and excitation spectra of the PL. At room temperature, glow curves of thermally stimulated luminescence (TSL) were recorded using a TLD reader I1009 that was supplied by Nucleonix Sys. Pvt. Ltd in Hyderabad. In the course of the TL test, the phosphor was subjected to UV light coming from a source emitting 254 nm of UV.[9,24,25,35]

3. Results and discussion

3.1 X-ray diffraction

The crystalline phase considerably affects the probability of both radiative and non-radiative decay processes due to the inter-ionic distance and the role of the crystalline behaviour in energy transfer. The XRD result for nano phosphor CaY$_2$O$_4$:Eu^{3+}

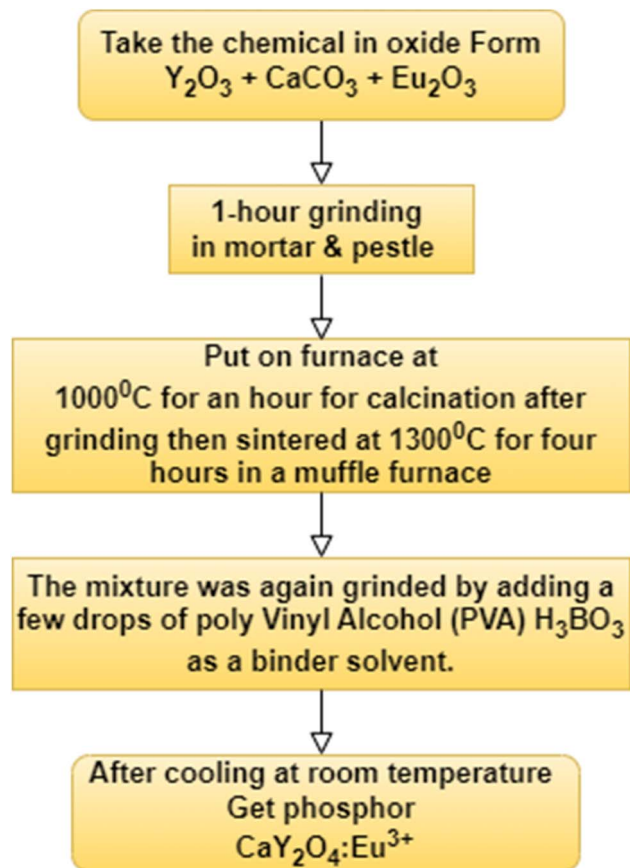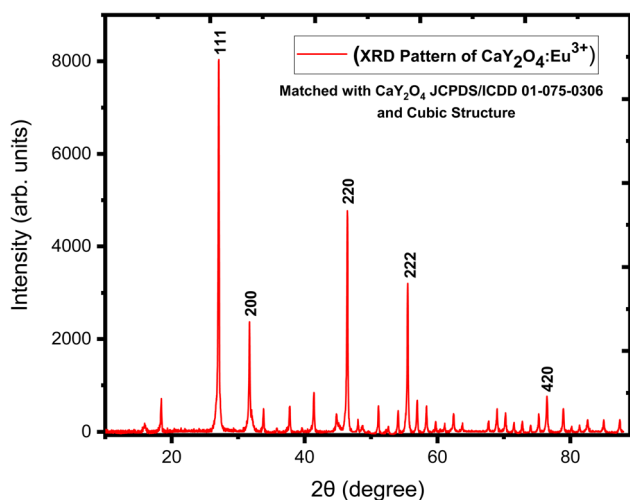Fig. 1 Flow chart of sample preparation.

Table 1 Calculation of crystallite size of $CaY_2O_4:Eu^{3+}$ phosphor

hkl	Peak position (2θ)	FWHM	Crystallite size D (nm)	Average size D (nm)
111	27.07759	0.19309	42.32714752	43.113
200	31.7155	0.21663	38.1304235	
220	46.44312	0.19783	43.70569803	
222	55.52602	0.19785	45.38561618	
420	76.4881	0.21986	46.01642362	

the nanopowders. A simple Debye–Scherrer's formula was used to determine a crystallite size that was estimated at 43.113 nm because full width at half maximum (FWHM) of the intense peak; they were matched to the JCPDS card number 01-075-0306.[24]

Scherrer's formula for the calculation of crystallite size is as follows:

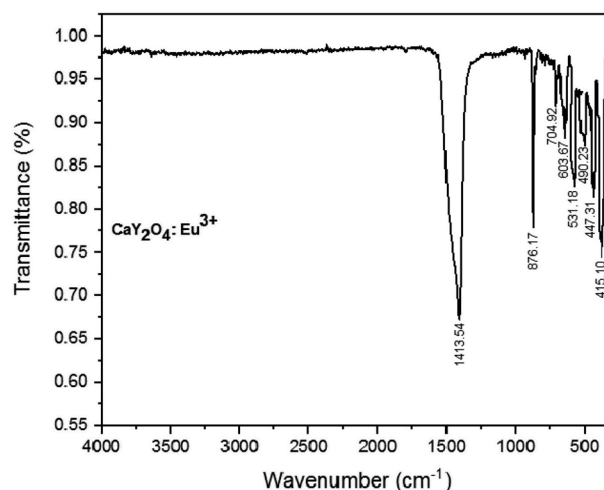$$D = \frac{0.9\lambda}{\beta \cos \theta}$$

In this context, the size of the crystallites is represented in this situation by the variable D. The FWHM is represented by the symbol β. The wavelength of the X-ray source is indicated by the symbol λ, while the diffraction angle is shown by the symbol θ. According to Table 1,

$$D = (0.9 \times 0.15409)/(\text{RADIANS}(0.19309) \times \text{COS}(\text{RADIANS}(27.07759)/2))$$

The average crystallite size is 43.113 nm.

3.2 Fourier transform-infrared spectroscopy (FTIR) analysis

The FTIR spectra of the Eu^{3+}-doped CaY_2O_4 phosphor are shown in Fig. 3. It is observed that strong peaks occur at 415–447 cm^{-1} which are a characteristic of the Y–O vibrations.[40] The medium sharp peak at 704 cm^{-1} corresponds to the O–Y–O

for (0.5–2.5 mol%) is shown in Fig. 2. At different values of 27.077, 31.715, 46.443, 55.526, and 76.488, five different peaks were obtained, which correspond to diffraction at the (111), (200), (220), (222), and (420) planes, respectively. In compliance with (JCPDS/ICDD 01-075-0306 & 00-019-0265), the spectrum indicates the predicted cubic structure crystalline process for

Fig. 2 XRD pattern of $CaY_2O_4:Eu^{3+}$.

Fig. 3 FTIR spectra of $CaY_2O_4:Eu^{3+}$.

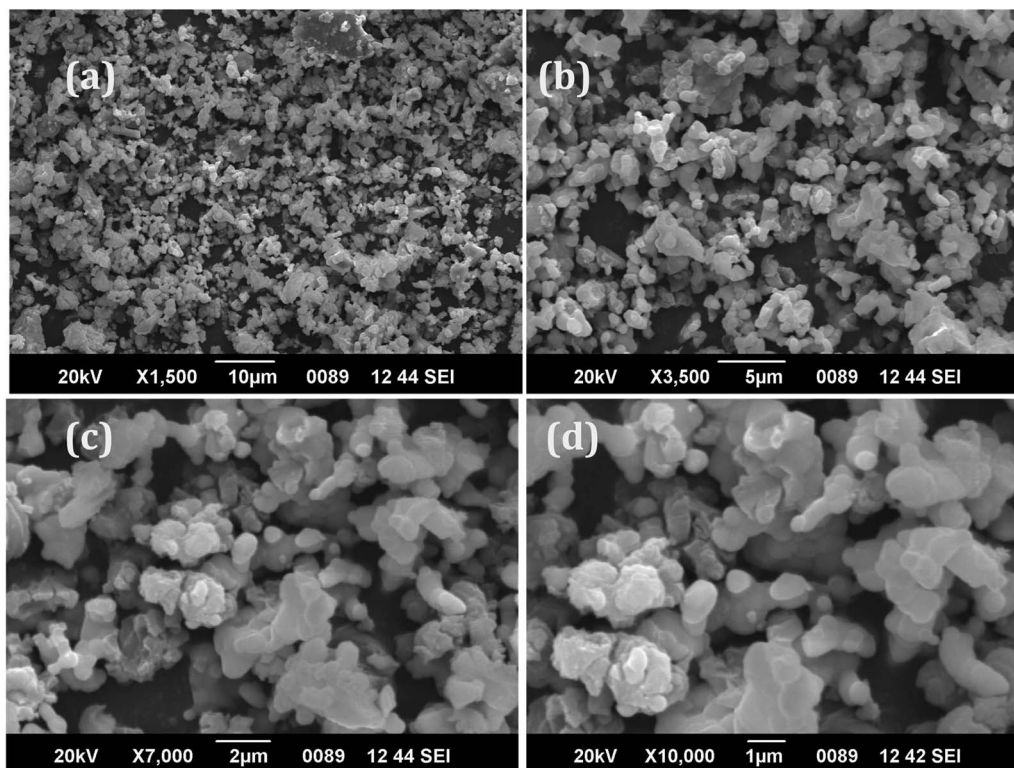**Fig. 4** (a–d) SEM images of phosphor CaY_2O_4-doped with of Eu^{3+} (2.5 mol%) ion prepared here.

deformation bond owing to the enlargement in the lattice of CaY_2O_4 after calcination. It can be noted that in the presence of O–Y–O, there is a vibration peak at 603 cm^{-1}, Y–O vibration at 531 cm^{-1}, and a stretching vibration at 490 cm^{-1}.[41,42] The sample showed a strong peak at 876 cm^{-1}, which was assigned to the formation of CaY_2O_4.[42]

3.3 SEM analysis

Fig. 4a–d show the SEM images collected under different resolutions of the Eu^{3+}(2.0 mol%)-doped CaY_2O_4 phosphor. From the images, the shape and size of the synthesised phosphors were studied. The diagram depicts a diverse morphology and noticeably large grain size.[23,26] The powders exhibit an uneven surface structure, indicating a propensity for grain growth and agglomeration at elevated temperatures. The distribution of grain sizes was wide, ranging from approximately 1 μm to 100 nm, with an average size falling within this range. Phosphor materials were synthesised at very high temperatures, which led to the formation of aggregates. The efficacy of luminescence may be reduced due to aggregation, which causes considerable dispersion of light. To increase the quality of phosphors and make them appropriate for use in solid-state lighting, a lengthy ball milling process is required to break up the aggregates. Here, at different resolutions of 1500–10 000×, the morphology of the phosphor exhibited a distinctive cubic structure, providing compelling evidence supporting the structural

analysis conducted on the synthesised phosphor using XRD analysis (Fig. 2).

3.4 Energy dispersive X-ray analysis (EDAX)

EDAX analysis can show the formation of elemental analysis in prepared phosphor. Fig. 5 shows an intense Ca (calcium) peak, an intense Y (yttrium) peak, and a peak from O (oxygen) with doping-ion Eu (europium), which confirmed that the phosphor was formed properly.

3.5 PL studies

The excitation and emission spectra of CaY_2O_4 phosphor doped with Eu^{3+} are depicted in Fig. 6a and b, which represent the oxide forms of inorganic elements. An excitation spectrum was observed at 613 nm, with a significant peak at 247 nm. Upon excitation, the phosphor emitted a broad range of wavelengths spanning from 535 to 631 nm, with notable high-intensity peaks at 613 and 631 nm resulting from energy transfers.

The excitation spectra of CaY_2O_4:Eu^{3+} phosphor were recorded by monitoring the Eu^{3+} $^5D_0 \rightarrow {}^7F_2$ transition at 613 nm. A large peak at 247 nm was seen in the excitation spectra, followed by another broad peak at 344 nm due to the $^7F_0 \rightarrow {}^5D_4$ transition. The maximum absorption intensity was observed at these two wavelengths. The excitation spectra (shown in Fig. 6a) included a prominent wide band with a peak at 247 nm, which is attributed to the charge transfer band (CTB) between Eu^{3+}
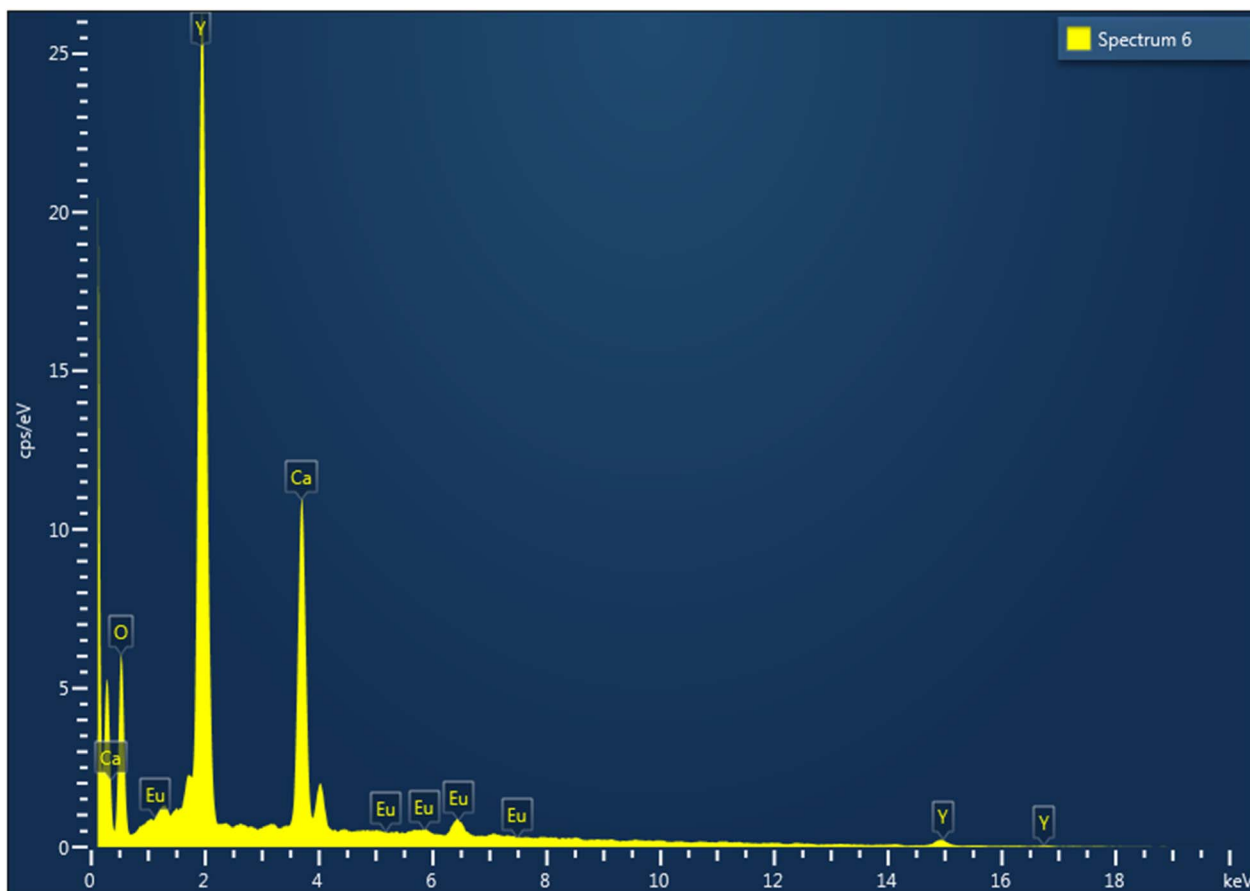
Fig. 5 EDAX analysis of the phosphor $CaY_2O_4:Eu^{3+}$ prepared here.

and O^{2-} neighbouring ions. Lines owing to the f–f transitions in the Eu^{3+} $4f^6$ arrangement were also seen at longer wavelengths.[29,30]

The emission spectrum of the phosphor was measured by exciting them with 247 nm, and the results are depicted in Fig. 6b. The spectrum comprises $^5D_0$–^7F_J ($J = 1$, 2, and 3) emission lines of Eu^{3+}. When Eu^{3+} occupies a crystallographic position devoid of inversion symmetry, the red-forced electric-dipole transition $^5D_0 \rightarrow {}^7F_2$ often dominates the emission spectrum. On the other hand, if the Eu^{3+} site has an inversion centre, the $^5D_0 \rightarrow {}^7F_1$ orange emission dominates.[31] The transitions from excited $^5D_0$ to the ^7F_J ($J = 0$–3) levels of Eu^{3+} ions produce distinctive emission lines within the 535–650 nm range. The placement of the Eu^{3+} ion in the CaY_2O_4 lattice, in combination with the selection criteria, determines the kind of transition from the emission levels to the terminating levels.[32,33,36–39]

The prominent peak at 613 nm is due to the electric dipole (ED) transition between the $^5D_0$ and $^7F_2$ levels, whereas the faint emission at 593 nm is due to a forced magnetic dipole (MD) transition process. The emission spectrum of the $CaY_2O_4:Eu^{3+}$ sample displays peaks ranging from 535–650 nm, which arise from the $^5D_0 \rightarrow {}^7F_J$ ($J = 1$, 2) transitions of Eu^{3+} ions upon excitation at 247 nm. The 535 nm, 613 nm, and 631 nm

peaks are attributed to the ED transition of $^5D_0 \rightarrow {}^7F_1$ and ($^5D_0 \rightarrow {}^7F_2$), respectively, with the 613 nm peak having twice the intensity of the 593 nm peak. The ratio of the 593 nm peak intensity to the 613 and 631 nm peaks is half, which differs from previous research findings. This suggests that the Eu^{3+} ions are located at a site with low symmetry in the CaY_2O_4 host, as the MD transition has a lower intensity than the ED transition. However, at a concentration of 2.0 mol% of Eu^{3+}, concentration quenching occurs as a consequence of energy transfer between Eu^{3+} ions, and the peak locations of the emission spectra alter. Therefore, the $CaY_2O_4:Eu^{3+}$ (2.0 mol%) phosphor could be a promising candidate for use in compact fluorescent lamps (CFLs) with excitation at 247 nm.

3.6 CIE coordinate

The peaks determined in spectrophotometry are put to the test by the CIE (Fig. 6c). Using a spectrophotometric technique and the spectrum energy distribution of the $CaY_2O_4:Eu^{3+}$ sample, the CIE coordinates were calculated (Fig. 6). The Eu^{3+}-doped sample has the colour coordinates of $x = 0.5169$ and $y = 0.4782$, which are near the orange-red spectrum of visible light. In accordance with the recommendations of the International Commission on Illumination (1931), a cross has been placed in the relevant area in Fig. 6c.[27,28,34]
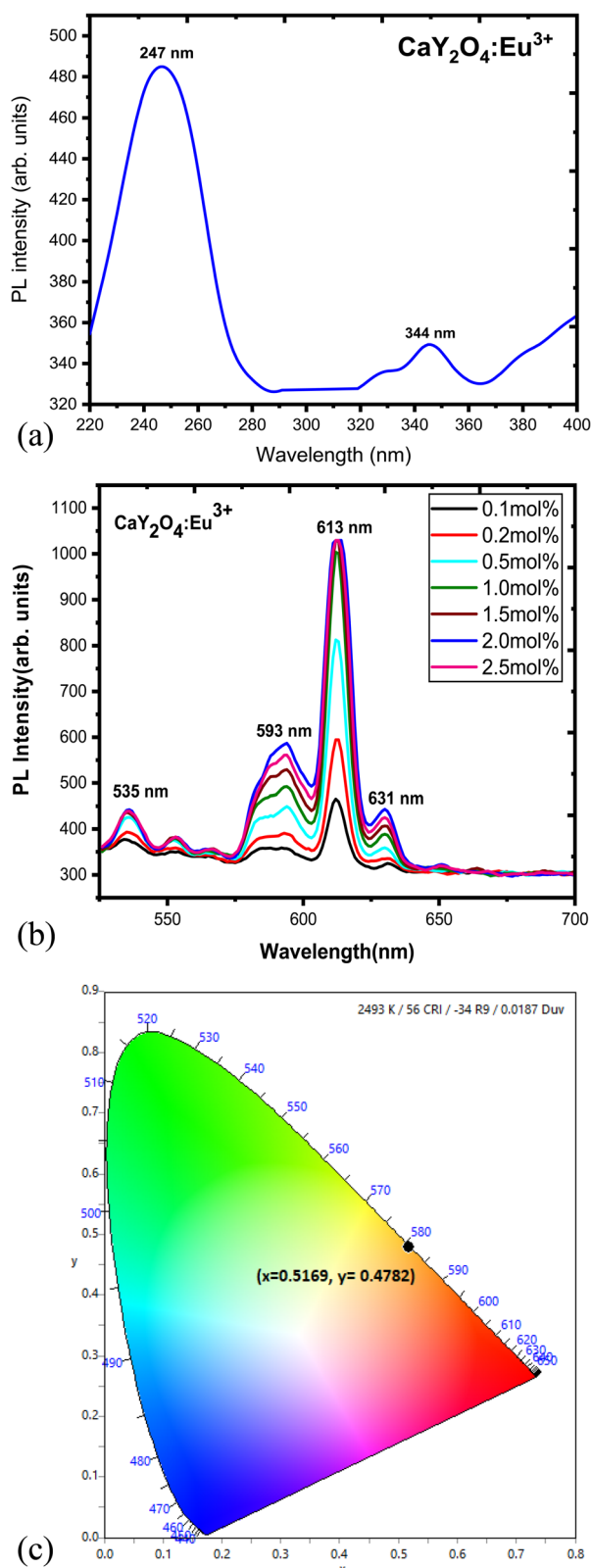
(a)

(b)

(c)

Fig. 6 (a) PL excitation spectra of $CaY_2O_4:Eu^{3+}$ at 2.0 mol%. (b) PL emission curve of $CaY_2O_4:Eu^{3+}$ for (0.1–2.5) mol%. (c) Commission Internationale de l'Eclairage (CIE 1931) of $CaY_2O_4:Eu^{3+}$ for 2.5 mol% ($x = 0.5169$, $y = 0.4782$).

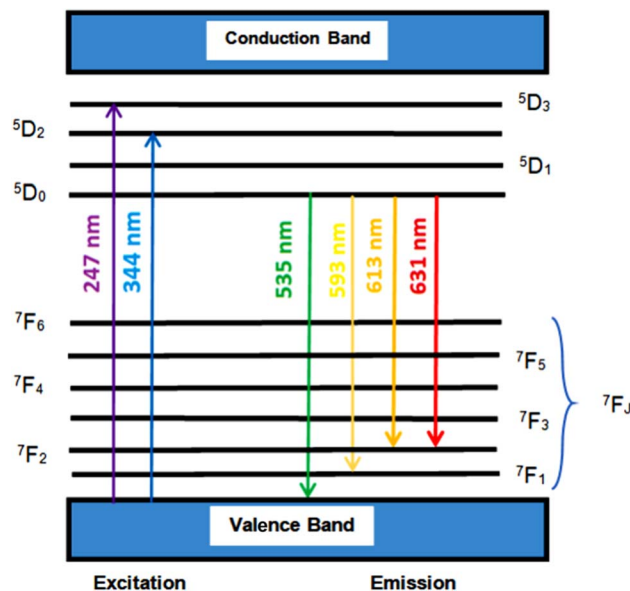**Fig. 7** Energy level diagram of $CaY_2O_4:Eu^{3+}$.

Fig. 7 shows the energy-level diagram of the Eu^{3+} ion in terms of the ED transition peak at 613 nm ($^5D_0 \rightarrow {}^7F_2$) and the dominant MD transition peak at 593 nm ($^5D_0 \rightarrow {}^7F_1$).

4. TL glow curve analysis

The TL glow curve of the $CaY_2O_4:Eu^{3+}$ phosphor illustrates a linear response to UV treatment at a constant heating rate of $6.7\ °C\ s^{-1}$ (Fig. 8). A good TL dosimeter peak can be seen at 225 °C as the TL intensity increases with UV exposure time (Fig. 8). This curve can be successfully theoretically and experimentally fitted using the CGCD method.

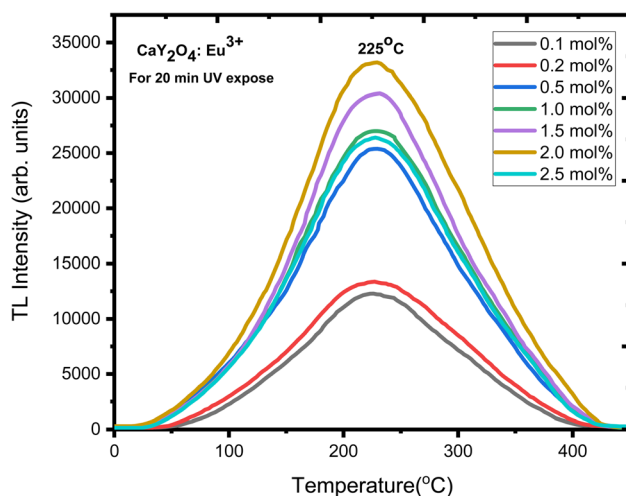Fig. 8 presents a distinct and wide TL glow curve with its peak centred at 225 °C. The intensity of the TL glow curve

Fig. 8 TL glow curve analysis of $CaY_2O_4:Eu^{3+}$.
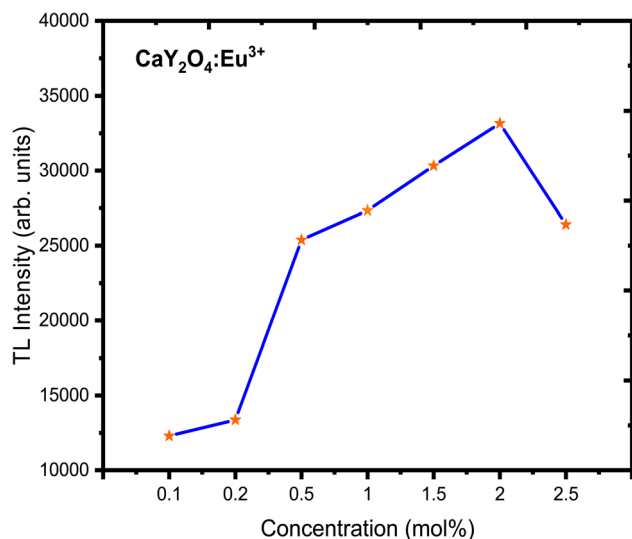
Fig. 9 $CaY_2O_4:Eu^{3+}$ concentration *vs.* intensity.

Fig. 11 $CaY_2O_4:Eu^{3+}$ phosphor TL glow curve dose *vs.* intensity plot.

demonstrates an upward trend as the concentration of doping ions increases, reaching its highest point at 2 mol%. Concentration quenching caused a loss of intensity after going over the highest point. This particular TL glow curve was obtained after a 20 minute exposure to UV radiation and is considered suitable for dosimetry applications. The concentration *versus* intensity plot is shown in Fig. 9 for better understanding.

As well-resolved broad TL glow curve was monitored in the dose *versus* intensity plot with various UV doses and 5–25 min UV exposure time (Fig. 10). Here, the intensity of the glow curve was measured at a fixed (optimised) concentration of 2.0 mol% of doping ion; it increased with increasing UV radiation exposure (Fig. 11). The well-resolved peak showed good linearity with the dose which showed the prepared phosphor could be useful for dosimetric applications.
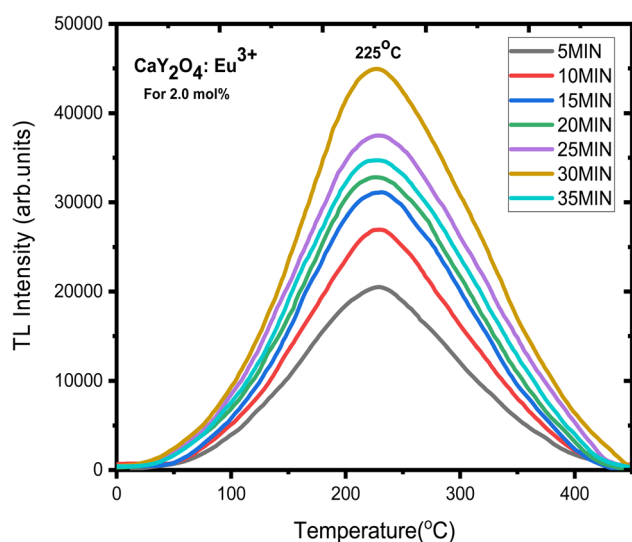

Fig. 12 CGCD of UV-induced $CaY_2O_4:Eu^{3+}$-doped phosphor for optimised UV dose and 2.0 mol% concentration.
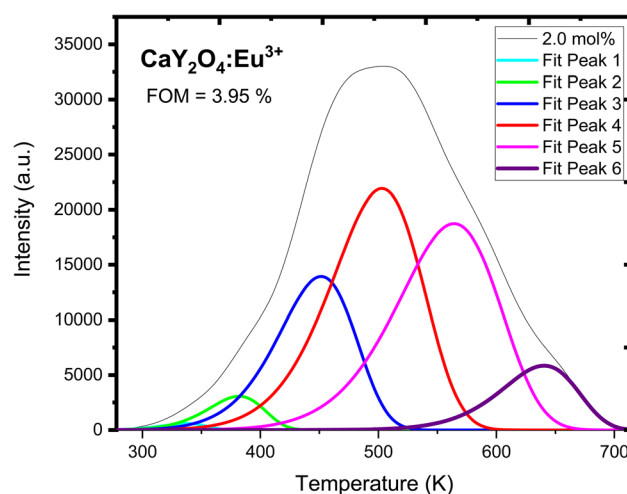
CGCD-fitted TL glow curves of $CaY_2O_4:Eu^{3+}$ phosphor (Fig. 12) that were exposed to UV radiation for 20 minutes are shown in Fig. 10. Table 2 displays a variety of trapping characteristics, including activation energy, order of kinetics, and frequency factors. After being exposed to UV light, the prepared sample's trap depth decreased from 0.5 to 1.0412 eV as shown by the fit, suggesting the creation of shallower traps. Irradiation by the UV rays from a lower energy source would have resulted in the formation of shallow trap levels, where electrons need less energy to tunnel through the barrier and recombine; hence, activation energy is lower for UV-irradiated samples. Fig. 12 shows the CGCD pattern of the optimised concentration (2 mol%) of the dopant with 25 min of UV exposure time; this pattern was composed of five distinct peaks, and Table 2 shows the calculated trap parameters of the CGCD pattern (a value of merit is 1.09%). It shows that the first order of kinetic and activation energies vary from 0.5 to 1.0412 eV, and the frequency

Fig. 10 TL glow curve analysis of $CaY_2O_4:Eu^{3+}$ for 2.0 mol%.

Table 2 Calculation of the kinetic parameters using the CGCD programme for UV-induced $CaY_2O_4:Eu^{3+}$-doped phosphor

T_1 (K)	T_m (K)	T_2 (K)	τ	δ	ω	$\mu = \delta/\omega$	Activation energy (eV)	Frequency factor (s^{-1})
311	338	359	27	21	48	0.4375	0.5	2.18×10^8
350	382	406	32	24	56	0.4285714	0.5001	2.14×10^8
406	452	485	46	33	79	0.4177215	0.5002	2.08×10^8
452	503	543	51	40	91	0.4395604	0.5275	2.31×10^8
505	564	608	59	44	103	0.4271845	0.5902	2.52×10^8
597	640	673	43	33	76	0.4342105	1.0412	4.52×10^8

factor values are very high, *i.e.*, 4.52×10^8 s^{-1} for the second fitted peak.

5. Conclusion

$CaY_2O_4:Eu^{3+}$ is a newly synthesised phosphor; the XRD analysis confirmed the existence of a single cubic crystalline phase with nanocrystalline behaviour. The surface morphology of the prepared phosphors was fine with a cube-like shape. Some vibration modes of Y–O, Ca–O, and Eu–O were observed in the FTIR spectra. Broad excitation for photoluminescence may be shown in the spectra with maxima at 247 and 344 nm. In the 247 nm-excited emission spectra, peaks at 535 nm, 593 nm, 613 nm, and 631 nm could be seen clearly, and the emission peaks were found to have corresponding transitions at 535 nm ($^5D_0 \rightarrow {}^7F_0$) and 593 nm ($^5D_0 \rightarrow {}^7F_1$), where the strongest peak was observed at 613 nm ($^5D_0 \rightarrow {}^7F_2$) and 631 nm ($^5D_0 \rightarrow {}^7F_2$). As a result, the phosphor exhibits remarkable colour constancy throughout its emission of light in the orange-to-red spectrum. The TL glow curve showed that the intensity of thermoluminescence increases with increasing UV exposure time and peaks at 225 °C, showing a good TL dosimeter peak. The kinetic parameters that were calculated for $CaY_2O_4:Eu^{3+}$ phosphor by the CGCD technique were fitted using the CGCD technique, which resulted in a successful theoretical and experimental fit[16] (Table 2).

Conflicts of interest

There are no conflicts to declare.

References

1 F. Clabau, X. Rocquefelte, S. Jobic, M. H. Whangbo, *et al.*, *Chem. Mater.*, 2005, **17**(15), 3904–3912.

2 Y. Li, M. Gecevicius and J. Qiu, *Chem. Soc. Rev.*, 2016, **45**(8), 2090–2136.

3 Y. Liu, B. Lei and C. Shi, *Chem. Mater.*, 2005, **17**(8), 2108–2113.

4 B. Liu, C. Shi and Z. Qi, *Appl. Phys. Lett.*, 2005, **86**(19), 191111.

5 J. Zhong, J. Chen, Q. Yang, C. Hu, J. Li and R. Duan, *Appl. Phys. A: Mater. Sci. Process.*, 2018, 124.

6 F. Clabau, X. Rocquefelte, T. Le Mercier, P. Deniard, S. Jobic and M. H. Whangbo, *Chem. Mater.*, 2006, **18**(14), 3212–3220.

7 D. Jia and W. M. Yen, *J. Lumin.*, 2003, **101**(1), 115–121.

8 J. Kuang, Y. Liu and J. Zhang, *J. Solid State Chem.*, 2006, **179**(1), 266–269.

9 J. Qiu and K. Hirao, *Solid State Commun.*, 1998, **106**(12), 795–798.

10 B. Zhang, X. Yu, T. Wang, S. Cheng, J. Qiu and X. Xu, *J. Am. Ceram. Soc.*, 2015, **98**(1), 171–177.

11 F. Liu, W. Yan, Y.-J. Chuang, Z. Zhen, J. Xie and Z. Pan, *Sci. Rep.*, 2013, **3**, 1554.

12 A. S. Pradhan and R. C. Bhatt, *Phys. Status Solidi A*, 1981, **68**(2), 405–411.

13 Y. Liu, J. Kuang, B. Lei and C. Shi, *J. Mater. Chem.*, 2005, **15**(37), 4025–4031.

14 K. Van den Eeckhout, P. F. Smet and D. Poelman, *Materials*, 2010, **3**(4), 2536–2566.

15 T. Wang, J. Gou, X. Xu, D. Zhou, J. Qiu and X. Yu, *Opt. Express*, 2015, **23**(10), 12595–12604.

16 Y. Parganiha, J. Kaur, V. Dubey and K. V. R. Murthy, *Mater. Sci. Semicond. Process.*, 2015, **31**, 715–719.

17 V. Dubey, J. Kaur, S. Agrawal, N. S. Suryanarayana and K. V. R. Murthy, *Superlattices Microstruct.*, 2014, **67**, 156–171.

18 P. Tadge, I. R. Martín, S. B. Rai, S. Sapra, T. M. Chen, V. Lavín, R. S. Yadav and S. Ray, *J. Lumin.*, 2022, **252**, 119261.

19 Y. S. Jeon, S. Hwangbo and K. S. Hwang, *J. Nanosci. Nanotechnol.*, 2019, **19**(3), 1709–1713.

20 K. S. Hwang, Y. S. Jeon, S. Hwangbo and J. T. Kim, *J. Nanosci. Nanotechnol.*, 2019, **19**(4), 2431–2434.

21 A. R. Krasnaya, B. M. Nosenko, L. S. Revzin and V. Y. Yaskolko, *Sov. Atom. Energy*, 1962, **10**, 625–626.

22 B. E. Bjärngard, J.-S. Tsai, R. K. Rice and B. E. Bjarngard, *Radiat. Res.*, 1989, **118**, 195.

23 T. Yamashita, N. Nada, H. Onishi and S. Kitamura, *Health Phys.*, 1971, **21**, 295–300.

24 R. Tamrakar, D. Bisen, K. Upadhyay and N. Bramhe, *Superlattices Microstruct.*, 2015, **81**, 34–48.

25 S. Ghorpade, R. Hari Krishna, R. Melavanki, V. Dubey and N. Patil, *Optik*, 2020, **208**, 164533.

26 J. Kaur, Y. Parganiha, V. Dubey, D. Singh and D. Chandrakar, *Superlattices Microstruct.*, 2014, **73**, 38–53.

27 V. Dubey and N. S. Suryanarayana, *J. Miner. Mater. Charact. Eng.*, 2010, **9**(12), 1101–1111.

28 V. Dubey, J. Kaur, N. S. Suryanarayana and K. V. R. Murthy, *Res. Chem. Intermed.*, 2013, **39**, 3689–3697.

29 G. R. Dillip, S. J. Dhoble, L. Manoj, C. M. Reddy and B. D. Raju, *J. Lumin.*, 2012, **132**, 3072.

30 K. N. Shinde, S. J. Dhoble and A. Kumar, *J. Rare Earths*, 2011, **29**, 527.

31 K. G. Lee, B.-Y. Yu, C.-H. Pyun and S.-I. Mho, *Solid State Commun.*, 2002, **122**, 485–488.

32 V. Dubey, J. Kaur, S. Agrawal, N. S. Suryanarayana and K. V. R. Murthy, *Superlattices Microstruct.*, 2014, **67**, 156–171.

33 M. R. Rao, *et al.*, PL Studies of Eu Doped YPO$_4$ Phosphor, *Proc. of NCAPMS*, 2013, pp. 212–213.

34 A. N. Yerpude and S. J. Dhoble, Luminescence Properties and Concentration Quenching of Sr$_5$SiO$_4$Cl$_6$:Eu^{3+} Phosphor, *Proc. of NCAPMS*, 2013, pp. 157–159.

35 S. Shigeo and M. William, *Phosphor Handbook*, CRC Press, Washington, D.C., 1998.

36 S. Lu and J. Zhang, *J. Lumin.*, 2007, **122–123**, 500–502.

37 P. A. M. Berdowski, J. VanKeulen and G. Blasse, *J. Solid State Chem.*, 1986, **63**, 86.

38 X. Zhang and H. J. Seo, *J. Alloys Compd.*, 2010, **503**, L14.

39 V. Dubey, J. Kaur and S. Agrawal, *Mater. Sci. Semicond. Process.*, 2015, **31**, 27–37.

40 P. Apte, H. Burke and H. Pickup, Synthesis of yttrium aluminum garnet by reverse strike precipitation, *J. Mater. Res.*, 1992, **7**, 706–711.

41 M. Maheshwary, B. P. Singh and R. A. Singh, *New J. Chem.*, 2015, **39**, 4494–4507.

42 M. Chroma, J. Pinkas, I. Pakutinskiene, A. Beganskiene and A. Kareiva, *Ceram. Int.*, 2005, **31**, 1123–1130.